Bisretinoids mediate light sensitivity resulting in photoreceptor cell degeneration in mice lacking the receptor tyrosine kinase Mer

Received for publication, September 20, 2018, and in revised form, October 19, 2018 Published, Papers in Press, October 23, 2018, DOI 10.1074/jbc.RA118.005949

Jin Zhao[‡], Keiko Ueda[‡], Marina Riera[‡1], Hye Jin Kim[‡], and Janet R. Sparrow[‡§2]

From the Departments of [‡]Ophthalmology and [§]Pathology and Cell Biology, Columbia University Medical Center, New York, New York 10032

Edited by George M. Carman

The receptor tyrosine kinase Mer is expressed by retinal pigment epithelial (RPE) cells and participates in photoreceptor outer-segment phagocytosis, a process enabling membrane renewal. Mutations in the gene encoding MERTK cause blinding retinitis pigmentosa in humans. Targeted *Mertk* disruption in mice causes defective RPE-mediated phagocytosis of the outer segments, leading to deposition of autofluorescent debris at the RPE–photoreceptor cell interface, followed by photoreceptor cell degeneration. Here, we show that retinaldehyde adducts (bisretinoid fluorophores) that form in photoreceptor outer segments occupy the unphagocytosed outer-segment debris that accumulates in *Mertk*$^{-/-}$ mice. Bisretinoids measured by HPLC were elevated in *Mertk*$^{-/-}$ mice compared with WT animals. Bisretinoids were also more abundant in albino *Mertk*$^{-/-}$ mice expressing leucine at position 450 of the isomerase RPE65 (Rpe65-Leu450) rather than the variant methionine (Rpe65-450Met) that yields lower bisretinoid levels. In Royal College of Surgeons rats having dysfunctional *Mertk*, bisretinoids were higher than in WT rats. Intensities of *in vivo* fundus autofluorescence were higher in *Mertk*$^{-/-}$ mice than in WT mice and peaked earlier in albino *Mertk*$^{-/-}$/Rpe65-Leu450 mice than in albino *Mertk*$^{-/-}$/Rpe65-450Met mice. Of note, the rate of photoreceptor cell degeneration was more rapid in albino *Mertk*$^{-/-}$ mice exposed to higher levels of intraocular light (albino *versus* pigmented mice) and in mice carrying Rpe65-Leu450 than in Rpe65-450Met mice, revealing a link between bisretinoid accumulation and light-mediated acceleration of photoreceptor cell degeneration. In conclusion, the light sensitivity of photoreceptor cell degeneration arising from *Mertk* deficiency is consistent with the known phototoxicity of bisretinoids.

Mice homozygous for a targeted deletion of the Mer receptor tyrosine kinase gene (*mer*^{kd}; *Mertk*$^{-/-}$) (1, 2), mice carrying a chemically induced point mutation in *Mertk* (3), and rats having a loss of function in *Mertk* (Royal College of Surgeons (RCS)[3] rats) (4, 5) exhibit recessively inherited progressive degeneration of photoreceptor cells. *Mertk* is expressed by retinal pigment epithelial cells (RPE), and the loss of photoreceptor cells is caused by an inability of the RPE to phagocytize the outer-segment disc membrane that is shed daily by the photoreceptors. The unphagocytosed outer-segment debris accumulates as autofluorescent extracellular debris at the RPE–photoreceptor outer-segment interface in the subretinal space (2, 4, 6–10). Early on, studies in the RCS rat assigned the defect to the RPE cell by employing chimeric animals (11) and RPE transplantation paradigms (12), and the disease-causing mutation in *Mertk* was identified by positional cloning (13). RPE culture systems demonstrated that *Mertk* functions in the ingestion phase of outer-segment phagocytosis (14). Transfer of WT *Mertk* to the RPE of RCS rats by viral vector reversed the ingestion defect and served to rescue the photoreceptor cells (15). Mutations in *MERTK* have also been identified in human subjects with retinitis pigmentosa (16), and although uncommon, these mutations are associated with abnormal patterns of fundus autofluorescence that include areas of increased autofluorescence intensity (17, 18).

In the presence of *Mertk* deficiency, electroretinographic recordings can be obtained until degeneration begins at ~3 weeks of age in the pink-eyed RCS rat (4, 6), with the debris zone becoming apparent at about postnatal day 12. Between 20 and 35 days of age, the volume of this material increases by ~30% (6). Loss of the photoreceptor cells in both the mouse and rat models is reflected in thinning of the outer nuclear layer (ONL); in the pink-eyed tan hooded RCS rats, ONL thickness is reduced by 50% at 1 month of age (6). In the RCS rat, the degeneration proceeds most rapidly in the central part of the retina and progresses toward the periphery with time (6). In the pink-

This work was supported in whole or in part by National Institutes of Health Grant EY12951 (to J. R. S.) and by unrestricted funds from Research to Prevent Blindness (to the Department of Ophthalmology, Columbia University). The authors declare that they have no conflicts of interest with the contents of this article. The content is solely the responsibility of the authors and does not necessarily represent the official views of the National Institutes of Health.

[1] Present address: Genetics Dept., Institute of Ocular Microsurgery, 08035 Barcelona, Spain.

[2] To whom correspondence should be addressed: Dept. of Ophthalmology, Columbia University, 635 W. 165th St., New York, NY 10032. Tel.: 212-305-9944; E-mail: jrs88@columbia.edu.

[3] The abbreviations used are: RCS, Royal College of Surgeons; RPE, retinal pigment epithelial cells; OCT, optical coherence tomography; ONH, optic nerve head; ONL, outer nuclear layer; qAF, quantitative fundus autofluorescence; UPLC, ultra-performance liquid chromatography; PE, phosphatidylethanolamine; H&E, hematoxylin and eosin; DAPI, 4′,6-diamidino-2-phenylindole; ANOVA, analysis of variance; SW-AF, short-wavelength fundus autofluorescence; NIR-AF, near-infrared fundus autofluorescence; NRPE, *N*-retinylidene-PE; *Rt*, retention time; GL, gray level; atRAL dimer, all-*trans*-retinal dimer.

eyed and albino rats, the outer-segment debris begins to disappear in posterior central retina at around postnatal day 55, and by day 96, most is gone posteriorly.

In healthy and diseased retina, autofluorescent vitamin A–aldehyde adducts that form in photoreceptor outer segments belong to the bisretinoid family of compounds that are internalized by RPE within phagocytosed outer-segment membranes. These fluorophores constitute the lipofuscin of RPE. The long-wavelength autofluorescence exhibited by bisretinoids is readily explained by the extensive systems of conjugated double bonds that populate the vitamin A–aldehyde (A2)-derived side arms of the molecules. The bisretinoid pigments of RPE lipofuscin in humans and rodents include A2E, iso-A2E, all-*trans*-retinal dimer, A2GPE, and all-*trans*-retinal dimer–phosphatidylethanolamine (19–28). The biosynthesis of bisretinoid occurs in photoreceptor outer segments with nonenzymatic condensation reactions between all-*trans*-retinaldehyde and phosphatidylethanolamine; the 11-*cis* isomer of retinaldehyde is the light-absorbing chromophore of rhodopsin. For the biosynthesis of A2E, the best known of the bisretinoid fluorophores, the immediate precursor is the phosphatidyl-pyridinium compound A2PE that we have identified in isolated photoreceptor outer segments (29, 30). The amount of bisretinoid in healthy photoreceptor cells is not normally sufficient to make an appreciable contribution to fundus autofluorescence because these compounds are continuously transferred to RPE cells through the process of outer-segment shedding and RPE phagocytosis.

Bisretinoids are photoreactive molecules that absorb light in the visible range of the spectrum and generate reactive forms of oxygen (23, 26, 31–35). Evidence derived from fluorescence spectra, age-associated accumulations, and disease phenotypes has shown that fundus autofluorescence in mice and humans originates primarily from bisretinoid lipofuscin in RPE cells. For instance, in both humans and mice, RPE lipofuscin (30, 36–39) and fundus autofluorescence (40–43) increase with age. RPE bisretinoid lipofuscin together with fundus autofluorescence also increases with ABCA4 deficiency in humans (44–46) and mice (24, 47). The spectral characteristics of the fluorescence emission generated from bisretinoid lipofuscin in mice are similar to the fundus autofluorescence spectra recorded noninvasively in humans (19, 48).

The outer-segment debris that accumulates in the RCS rat retina is considered to figure prominently in events leading to photoreceptor cell degeneration, and although the precise mechanisms are not known, several processes have been proposed. For instance, the debris has been suggested to serve as a diffusion barrier (49), as a cause of vitamin A deficiency (50), as a disruption of the interphotoreceptor matrix (51) and cyclic nucleotide metabolism (52), and as a source of hydrolases (53). However, these mechanisms do not address the composition of the outer-segment debris or its ability to confer light sensitivity.

The *Mertk*$^{-/-}$ mouse provides an excellent platform for assessing the impact of bisretinoids on the health of the photoreceptor cells in which they form. To examine the molecular composition of the outer-segment debris and to explore the cause of photoreceptor cell degeneration in the presence of *Mertk* mutations, we generated mice carrying null mutations in *Mertk* in albino and pigmented mice and in mice carrying the Rpe65 amino acid variant (leucine or methionine at residue 450) that confers different levels of bisretinoid formation (22). Here, we demonstrate that bisretinoid fluorophores are the source of autofluorescence in the photoreceptor cell debris that accumulates in *Mertk*$^{-/-}$ mice, and we provide evidence that these photoreactive compounds are linked to mechanisms whereby light aggravates photoreceptor cell degeneration in the *Mertk*$^{-/-}$ mouse.

Results

In vivo fundus autofluorescence

We imaged *in vivo* fundus autofluorescence noninvasively using instrumentation comparable with that used clinically. Fundus autofluorescence captured using 488-nm excitation (short-wavelength fundus autofluorescence; SW-AF) originates primarily from the bisretinoids that are amassed in retina as lipofuscin (48). With SW-AF imaging of *Mertk*$^{-/-}$ mice at 4 and 5 weeks of age, the fundus appeared relatively uniform in all mice (54 images, 27 mice) (Fig. 1*A*). At 6 weeks of age in the albino *Mertk*$^{-/-}$ mice (8 of 9 Rpe65-450Met; 8 of 8 Rpe65-Leu450), dark and bright mottling of the fundus was visible. Dark patchiness was even more pronounced in the albino *Mertk*$^{-/-}$/Rpe65-Leu450 mice (10 of 12) at 8 weeks, whereas in the agouti *Mertk*$^{-/-}$/Rpe65-450Met mice (6 of 6), distinct areas of hyperautofluorescence were observed inferiorly (Fig. 1*A*). In all (10 of 10) albino *Mertk*$^{-/-}$/Rpe65-Leu450 mice at 12 weeks of age, the optic nerve head (ONH) and vasculature were noticeably indistinct. Hyperautofluorescent puncta were also a feature of the SW-AF images in all mouse lines beginning as early as 8 weeks of age; because ocular pigmentation provides a dark background, the puncta were particularly pronounced in agouti *Mertk*$^{-/-}$/Rpe65-450Met mice and in some eyes persisted at ages of 12 (Fig. 1*A*), 15 (not shown), and 24 (Fig. 1*B*) weeks. NIR-AF imaging in the agouti *Mertk*$^{-/-}$/Rpe65-450Met mice revealed that the hyperautofluorescent puncta in these mice were also visible as bright spots in NIR-AF images (Fig. 1*B*). Whether a given quadrant was affected earlier by patchy nonuniformities was difficult to ascertain, but affected areas typically included posterior central retina. The hyperautofluorescent spots became visible before the appearance of darkened patches, and when central hypoautofluorescence dominated central fundus, autofluorescent spots were still visible peripherally. Note that in some images, fundus autofluorescence photographs in the *Mertk*$^{-/-}$ mice could appear equally bright across ages and genotypes; however, darkening of the internal autofluorescent reference in these cases (*rectangle* at the *top* of the image) was a sign that a shorter exposure was sufficient to image the higher fundus SW-AF levels in the mice.

Bisretinoid lipofuscin was measured *in vivo* by quantifying SW-AF intensities (quantitative fundus autofluorescence, qAF) as reported previously (43). In the albino *Mertk*$^{-/-}$/Rpe65-Leu450 mice, qAF reached a peak at age 6 weeks, whereas in *Mertk*$^{-/-}$/Rpe65-450Met mice, qAF peaked at age 10 weeks; otherwise, the values were essentially at baseline (Fig. 1*C*). Because SW-AF intensities are modified by the presence or absence of melanin (54), absolute levels of qAF in the albino

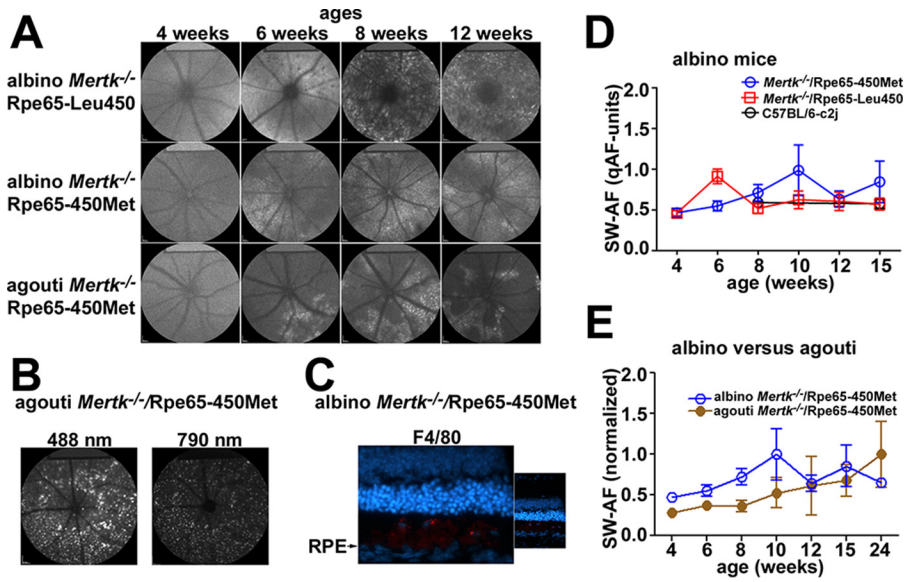

Figure 1. Fundus AF (488 and 787 nm) in *Mertk*$^{-/-}$ and WT mice varying in the Rpe65-L450M variant and in melanin content (albino and agouti). *A*, SW-AF fundus images (488-nm excitation) acquired from *Mertk*$^{-/-}$ mice at the ages indicated. Autofluorescent puncta are more visible in the agouti mice due to ocular pigmentation. *B*, SW-AF (488 nm) and NIR-AF (790 nm) images (age 24 weeks). Autofluorescent spots in SW-AF are also detectable in NIR-AF images. *C*, cryostat section stained with antibody to F4/80, a label specific for macrophages (albino *Mertk*$^{-/-}$/Rpe65-Leu450, age 6 weeks). The micrograph captured 0.5–1 mm from the optic nerve head. *D* and *E*, qAF (488-nm excitation). For quantitation, mean GLs were determined in eight circularly arranged segments located 8.25–19.25° from the disc center and were standardized to GL values determined for the internal fluorescent reference (*rectangular area* at *top* of image) to calculate qAF. In *E*, qAF of albino and agouti mice were normalized to a maximum value of 1. Values are mean ± S.D. (*error bars*). In some cases, error bars do not extend further than the height of the *symbol*.

Mertk$^{-/-}$/Rpe65-450Met mice relative to qAF in the agouti *Mertk*$^{-/-}$/Rpe65-450Met mice could not be compared. Nevertheless, mean qAF normalized to a maximum value of 1 showed that in the latter agouti mice, fundus autofluorescence appeared to undergo a steady climb from age 4 to 24 weeks; the values at 4, 6, and 8 weeks were significantly different from that at age 24 weeks ($p < 0.05$, one-way ANOVA with Tukey's multiple-comparison test), whereas qAF in the albino mice peaked at age 10 weeks (Fig. 1*D*).

As noted above, qAF in the albino *Mertk*$^{-/-}$/Rpe65-Leu450 mice peaked at 6 weeks of age. The decline in fundus AF that followed was visible in the fundus images (Fig. 1*A*) and evident in the plotted qAF values (Fig. 1*D*). This decrease can be accounted for by bleaching and resolution of the autofluorescent debris. Photoreceptor cells, the source of the AF, are also dying during this period (discussed below).

Fluorescence microscopy

To test for the presence of autofluorescence at the RPE–photoreceptor interface, as exhibited by RCS rats (7, 10), we examined cryostat (horizontal) sections that had been stained with DAPI to label nuclei (Fig. 2). As shown in Fig. 2, albino *Mertk*$^{-/-}$/Rpe65-Leu450 mice exhibited an inherent autofluorescence at the interface between RPE and photoreceptor cells when examined by fluorescence microscopy. The nuclei of the RPE monolayer were situated on the choroidal side of the autofluorescent band. The autofluorescence in the subretinal space was visible at 6 weeks of age in albino *Mertk*$^{-/-}$/Rpe65-Leu450 mice and in the albino *Mertk*$^{-/-}$/Rpe65-450Met mice, but in keeping with slower disease progression, it was not visible in agouti *Mertk*$^{-/-}$/Rpe65-450Met mice at this age. Muller cell processes are reported as being present in the photoreceptor

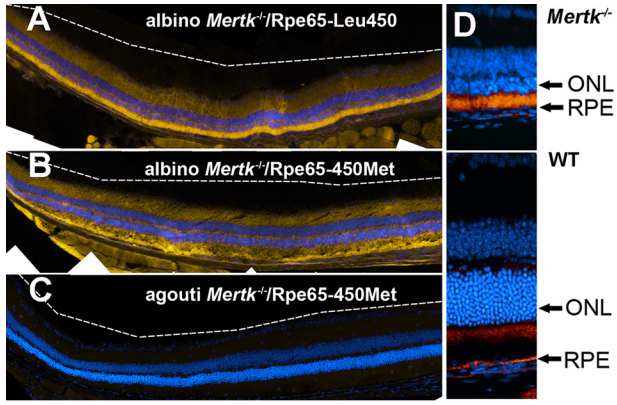

Figure 2. Fluorescence micrographs of inferior hemiretina of *Mertk*$^{-/-}$ mice. Shown are cryostat sections (10-μm thickness). *Blue*, DAPI fluorescence; *yellow/orange*, autofluorescence (excitation, 490 nm). Age was 6 weeks. *A*, albino *Mertk*$^{-/-}$/Rpe65-Leu450. *B*, albino *Mertk*$^{-/-}$/Rpe65-450Met. *C*, agouti *Mertk*$^{-/-}$/Rpe65-450Met. All exposure times (2 s) was chosen so as not to saturate the fluorescence in the albino *Mertk*$^{-/-}$/Rpe65-Leu450. *Brightness* in the image of albino WT (*D*) was increased to demonstrate AF in the RPE.

debris zone (55, 56); thus, uptake of the fluorescent molecules by Muller glia may account for the patterns of autofluorescence that appear to extend across the full thickness of neural retina, particularly in the albino *Mertk*$^{-/-}$/Rpe65-450Met mice.

UPLC analysis

A representative UPLC chromatogram in Fig. 3 shows the detection of bisretinoids in chloroform/methanol extracts of whole eyecups from albino *Mertk*$^{-/-}$/Rpe65-Leu450 mice (age 6 weeks) (35, 57). On the basis of UV-visible absorbance spectra (monitoring at 430 nm) and retention times, absorbance peaks analyzed by UPLC could be assigned to the fluorophores A2GPE (λ_{max} = 346 and 438 nm), all-*trans*-retinal dimer

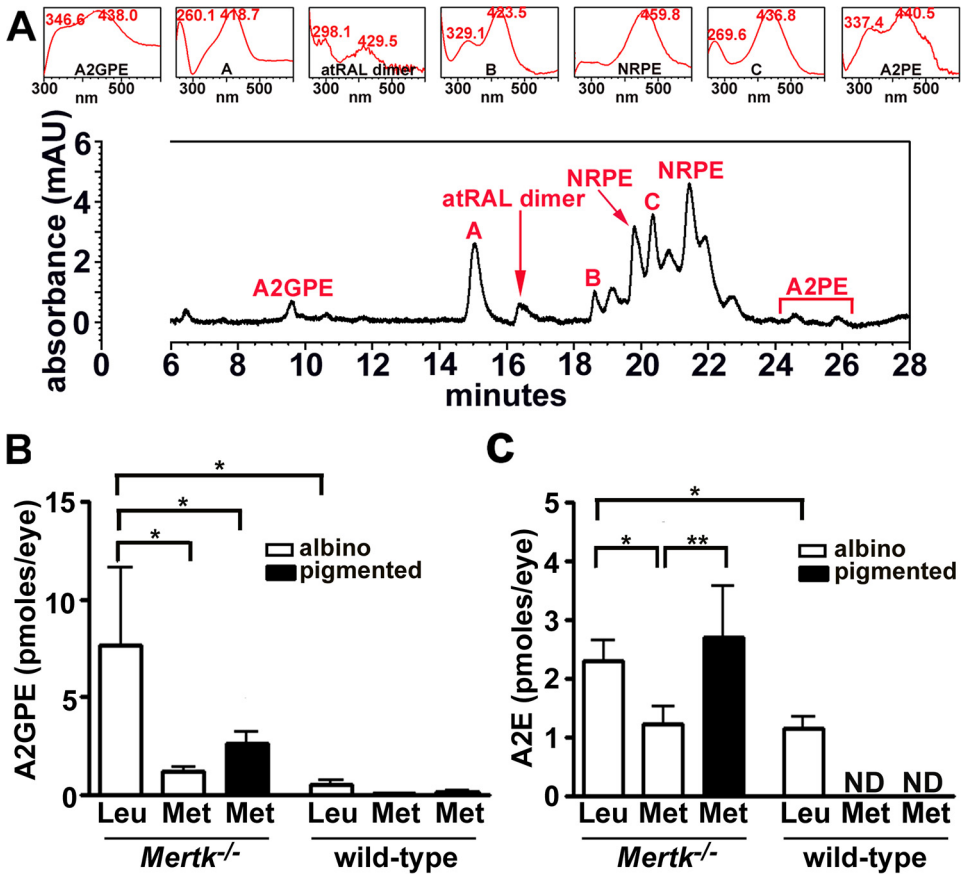

Figure 3. UPLC identification of bisretinoids in *Mertk*$^{-/-}$ mice. *A*, UPLC detection of A2GPE (*Rt* = 9.6 min), atRAL dimer (*Rt* = 16.4 min), NRPE (*Rt* = 19.8 and 20.9–22.0 min), and A2PE (*Rt* = 24.6 and 25.9 min) in albino *Mertk*$^{-/-}$/Rpe65-Leu450 at age 6 weeks. *Peaks A–C* have absorbance spectra consistent with oxidized bisretinoids. *Insets* at *top*, UV-visible absorbance spectra of chromatographic peaks corresponding to bisretinoids. 10 eyes/sample. Retention time is shown in minutes. *B* and *C*, measurement by reverse phase UPLC (A2GPE) and HPLC (A2E) at age 8 weeks. Values are means ± S.D. (*error bars*); 4–6 eyes (2–3 mice) were pooled for each sample; 2–9 independent samples/mean. *, $p < 0.05$; **, $p < 0.01$ determined by one-way ANOVA and Newman–Keuls comparison test. *mAU*, milli-absorbance units.

(λ_{max} = 298 and 429 nm), and A2PE (λ_{max} = 337 and 440 nm) (Fig. 3*A*). Two peaks attributable to PE-all-*trans*-retinal Schiff base adducts (*N*-retinylidene-PE; NRPE) varying in fatty acid composition are also present. Other peaks (*labeled A*, *B*, and *C*) having both UV and visible absorbance maxima (λ_{max} = 260 and 418 nm, 329 and 423 nm, and 269 and 436 nm), suggestive of oxidized bisretinoid fluorophores, were also present (Fig. 3). In UPLC profiles under the chromatographic conditions utilized for Fig. 3*A*, A2E would be expected to elute as an ill-defined peak at a retention time (*Rt*) of 6.8 min; this peak was not detected at age 6 weeks.

Quantitation by integrating peak areas revealed that A2GPE (quantified in UPLC profiles) and A2E (HPLC) levels were higher in albino *Mertk*$^{-/-}$/Rpe65-Leu450 mice as compared with WT at age 8 weeks ($p < 0.05$) (one-way ANOVA and Newman–Keuls multiple-comparison test); the difference between albino *Mertk*$^{-/-}$/Rpe65-Leu450 and albino *Mertk*$^{-/-}$/Rpe65-450Met mice was also statistically significant ($p < 0.05$) for both A2E and A2GPE.

Photoreceptor cell degeneration

Photoreceptor cell degeneration was readily detectable in H&E-stained paraffin sections of the eyes (Fig. 4). As shown previously in *mer*^{kd} mice (1, 2), photoreceptor cell degeneration

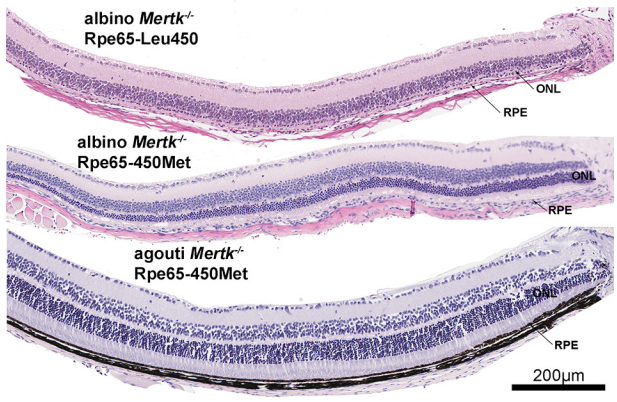

Figure 4. Representative light micrographs of inferior hemiretina of *Mertk*$^{-/-}$ mice varying in coat color and Rpe65-450 variant (age 8 weeks). H&E-stained sections are shown.

was indicated by reduced width of ONL. Specifically, ONL thinning was observed at 6 weeks of age in the albino *Mertk*$^{-/-}$/Rpe65-Leu450 mice and albino *Mertk*$^{-/-}$/Rpe65-450Met mice but was not noticeable in agouti *Mertk*$^{-/-}$/Rpe65-450Met (not shown). At 8 weeks of age in the albino *Mertk*$^{-/-}$/Rpe65-Leu450 mice, the ONL was reduced to only a single row of cell nuclei (Fig. 4). At the same age, ONL width was also visibly reduced in the albino *Mertk*$^{-/-}$/Rpe65-450Met mice (Figs. 4

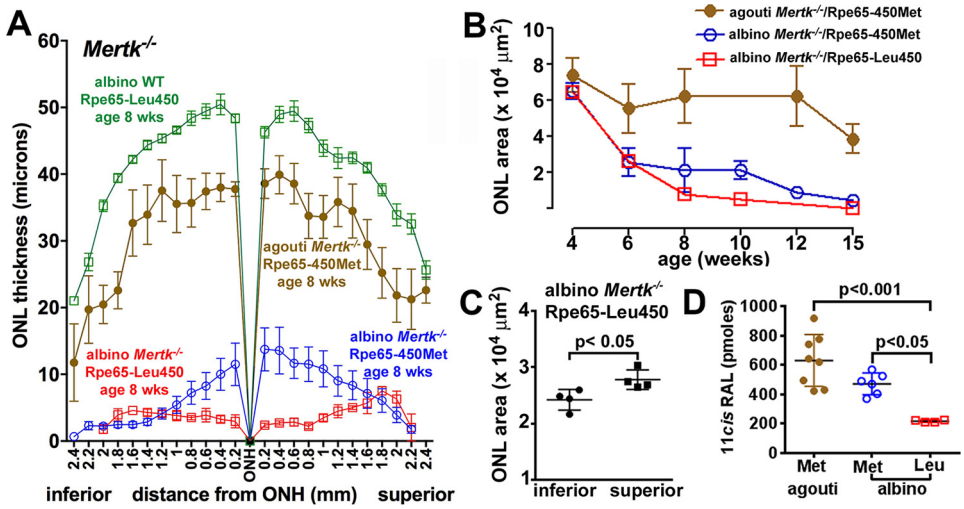

Figure 5. Photoreceptor cell viability measured as ONL thickness. *Mertk*$^{-/-}$ mice varying with respect to coat color (agouti, albino) and Rpe65-L450M variant. *A*, ONL thicknesses plotted as a function of distance from ONH in inferior and superior retina. Values are mean ± S.E. (*error bars*), 6–10 eyes. *B*, progression of photoreceptor cell degeneration plotted as decreasing ONL area with age (weeks). *C*, albino *Mertk*$^{-/-}$/Rpe65-Leu450 (age 6 weeks). ONL area was calculated from thicknesses measured 2 mm superior and inferior to the ONH. *D*, measurement of 11-*cis*-retinal in *Mertk*$^{-/-}$ mice. *Error bars* (*B–D*), S.D.

and 5) but to a lesser extent. The acidophilic subretinal debris zone was readily visible in H&E-stained sections acquired from the albino *Mertk*$^{-/-}$/Rpe65-450Met mice (Fig. 4). Photoreceptor cell viability was quantified in *Mertk*$^{-/-}$ mice by measuring ONL thickness. Plotting of ONL thickness as a function of distance superior and inferior to the optic nerve head in the vertical plane revealed that in all three *Mertk*$^{-/-}$ mouse lines, photoreceptor cell degeneration was detected as thinning of the ONL at 8 weeks of age (Fig. 5*A*). For comparative purposes, we calculated mean ONL area within the segments of retina extending from the ONH to a point 2 mm in the superior and inferior hemi-retina (Fig. 5*B*). The thinning was most rapid in the albino *Mertk*$^{-/-}$/Rpe65-Leu450 mice followed by the albino *Mertk*$^{-/-}$/Rpe65-450Met mice. The reduction in ONL thickness was slower in the agouti *Mertk*$^{-/-}$/Rpe65-450Met line. Growth of the mouse eyeball (estimated by measuring corneal diameter), with concomitant changes in photoreceptor cell density, reaches a plateau at ~8 weeks of age (58). At age 8 weeks, the percent difference (value 1 − value 2/mean value 1 + value 2 × 100%) between agouti *Mertk*$^{-/-}$/Rpe65-450Met mice and albino *Mertk*$^{-/-}$/Rpe65-450Met mice was 98% ($p <$ 0.05, one-way ANOVA and Sidak's multiple-comparison test), and the percentage difference between albino *Mertk*$^{-/-}$/Rpe65-Leu450 and albino *Mertk*$^{-/-}$/Rpe65-450Met mice was 92% ($p < 0.05$) (Fig. 5*B*).

To test for hemispheric differences in the *Mertk*$^{-/-}$, we compared ONL thinning in superior *versus* inferior retina in albino *Mertk*$^{-/-}$/Rpe65-Leu450, albino *Mertk*$^{-/-}$/Rpe65-450Met, and agouti *Mertk*$^{-/-}$/Rpe65-Leu450 mice at 6, 8, and 12 weeks, respectively. Whereas there was a trend toward faster ONL thinning in the inferior hemiretina of all three mouse lines, statistical significance was only reached in the albino *Mertk*$^{-/-}$/Rpe65-Leu450 mice at 6 weeks of age (Fig. 5*C*) (two-tailed *t* test), and this difference was no longer statistically significant at 8 weeks of age (data not shown).

Levels of 11-*cis*-retinal, an indicator of the numbers of viable photoreceptor cells (59), were also lower in the albino *Mertk*$^{-/-}$/Rpe65-Leu450 mice relative to the albino *Mertk*$^{-/-}$/Rpe65-450Met and agouti *Mertk*$^{-/-}$/Rpe65-450Met mice (age 8 weeks) (Fig. 5*D*) (one-way ANOVA and Tukey's multiple-comparison test); the differences were 29% ($p < 0.05$) and 98% ($p < 0.05$), respectively.

Chromatographic analysis of RCS rat

We also analyzed bisretinoids in chromatograms obtained from eyecups of pigmented and albino RCS rats (Fig. 6). HPLC and UPLC were both employed together with columns having different retention properties. Peak authentication was confirmed by UV-visible absorbance and retention times. By HPLC with a C4 column that favors A2PE and all-*trans*-retinal dimer elution (33), A2PE-attributable peaks were detected in samples obtained from the albino RCS rat while being absent in the albino RCS-rdy+ control rat (60) (Fig. 6*A*). The presence of A2E and iso-A2E in the analyte, albeit at low levels, is probably explained by the presence of a phospholipase D–like activity in outer segments (61).

As also demonstrated in the UPLC chromatograms presented in Fig. 6, the Schiff base adduct NRPE (62), which is a precursor in the bisretinoid biosynthetic pathway, presented as multiple pronounced peaks in the RCS rat samples while being less abundant in the WT Long Evans rat (Fig. 6*B*). NRPE presents as a series of peaks because of species of NRPE differing in fatty acid composition. A2PE and all-*trans*-retinal dimer were detected in the RCS rat while being absent in chromatograms associated with the Long Evans rat. The A2GPE peak (35) was also greater in the mutant rat.

Discussion

Mutations in *MERTK* have been identified in human subjects with retinitis pigmentosa and account for about 1% of nonsyndromic autosomal recessive cases (16, 63). These mutations in humans cause severe rod–cone degeneration (16, 64). Fundus autofluorescence images acquired from these individuals exhibit abnormal patterns that include hyperautofluorescent

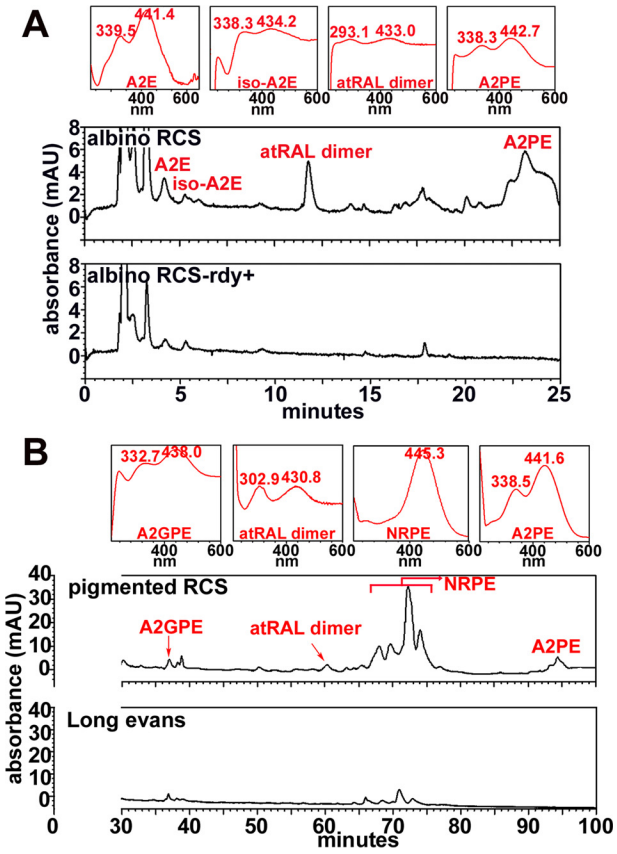

Figure 6. Representative chromatograms illustrating the detection of bisretinoid lipofuscin pigments in RCS rat eyecups. *A*, posterior eyecups from albino dystrophic RCS rats and control rats (RCS-rdy+) were analyzed by reverse-phase HPLC with a C4 column and monitoring at 430 nm (age 2 months). Compounds were identified on the basis of UV-visible absorbance and retention times recorded using authentic standards. Detection of A2E (*Rt* = 4.2 min), iso-A2E (*Rt* = 5.3 min), atRAL dimer (*Rt* = 11.8 min), and A2PE (*Rt* = 23.2 min). *B*, UPLC analysis of eyecups obtained from pigmented RCS rats and WT Long Evans rats (430-nm monitoring; age 2 months; detection of A2GPE (*Rt* = 37.0 min), atRAL dimer (*Rt* = 60.2 min), and A2PE (*Rt* = 94.3 min)). *Insets* (*top*), UV-visible absorbance spectra of chromatographic peaks corresponding to bisretinoids. *mAU*, milli-absorbance units.

puncta, mottling, increased central autofluorescence, and eventually macular atrophy marked by a pronounced reduction in autofluorescence (17, 18). Optical coherence tomography (OCT) reveals a loss of the ellipsoid hyperreflectivity layer; this alteration is attributable to photoreceptor cell degeneration (18). These disease-related features correspond well to the fundus and histometric changes that we observed in the *Mertk*$^{-/-}$ mice.

In color fluorescence micrographs (albino *Mertk*$^{-/-}$/Rpe65-Leu450 and albino *Mertk*$^{-/-}$/Rpe65-450Met mice), we observed golden-yellow autofluorescence (excitation, 490 nm) anterior to the RPE; this autofluorescence was consistent with the presence of the previously described debris zone in light microscopic images acquired from RCS rats and *Mertk*^{kd} mice (2, 4, 6, 65). In a clinically relevant approach, we also detected this autofluorescence by *in vivo* SW-AF imaging. Increased autofluorescence and mottling were observed, as with SW-AF imaging in human patients carrying mutations in *MERTK* (17, 18). Fundus AF intensity in albino *Mertk*$^{-/-}$/Rpe65-Leu450 mice peaked at 6 weeks of age, a time point that was earlier than in the other mouse lines and that was consistent with the faster rate of bisretinoid formation associated with expression of leucine at position 450 of Rpe65 (22). Conversely, the Rpe65-450Met variant expressed by C57BL/6J and C57BL/6J^{c2j} mice has been shown to slow the regeneration of 11-*cis*-retinal production (66, 67). The retarded kinetics in the presence of the methionine 450 substitution is also associated with reduced bisretinoid in albino C57BL/6J^{c2j} (Rpe65-450Met) *versus* BALB/cJ (WT Rpe65-Leu450) mice (22), reduced capacity for photon catch (67), and some resistance to light damage (66, 68, 69). Similarly, in the present studies, albino *Mertk*$^{-/-}$/Rpe65-450Met (age 8 weeks) mice expressed A2E and A2GPE levels that were lower than in the albino *Mertk*$^{-/-}$/Rpe65-Leu450 mice. The more rapid photoreceptor cell degeneration in the albino *Mertk*$^{-/-}$/Rpe65-Leu450 mice as opposed to the albino *Mertk*$^{-/-}$/Rpe65-450Met mice is indicative of a difference associated with bisretinoid levels. Chromatographic measurements of bisretinoid further showed that bisretinoids are elevated in RCS rat eyecups relative to RCS-rdy+ control rats.

It has been estimated that retinal irradiance in the albino is 2 orders of magnitude more than in pigmented eyes (70). It is thus significant that photoreceptor cell degeneration was also accelerated in the albino *Mertk*$^{-/-}$/Rpe65-450Met mice relative to the agouti *Mertk*$^{-/-}$/Rpe65-450Met mice, indicating that light modulates the degeneration. The difference in the timeline of photoreceptor cell degeneration due to ocular pigmentation probably also explains why normalized qAF peaked at 6 weeks in the albino *Mertk*$^{-/-}$/Rpe65-450Met mice while continuing to rise in the agouti *Mertk*$^{-/-}$/Rpe65-450Met mice. Reports of studies in the RCS rat also implicate light as a factor aggravating photoreceptor cell degeneration. For instance, RCS rats with pigmented eyes or RCS rats raised in darkness exhibit a slower rate of degeneration than cyclic-light–reared melanin-deficient RCS rats (4, 6, 71).

ONL thinning due to loss of photoreceptor cells also occurs more rapidly in inferior retina than in the superior hemisphere in both pigmented RCS rats (6) and pigmented *Mertk* null mutant mice (2). Similarly, we observed that ONL thinning occurred faster in the inferior hemiretina of albino *Mertk*$^{-/-}$/Rpe65-Leu450 mice. Here the difference was 14% at 6 weeks of age ($p < 0.05$). The propensity for light damage inferiorly in *Mertk* mutant mice is consistent with inferior damage observed in animals raised at elevated light levels (72), in transgenic mice expressing the P23H mutation (73), and in patients with sectoral retinitis pigmentosa (74). In many of these cases, the more rapid progression of disease in inferior retina is attributed to the modifying effects of light.

The light sensitivity expressed by *Mertk* mutant mice is readily accounted for by bisretinoid phototoxicity. Specifically, bisretinoids have the propensity to photogenerate reactive oxygen species such as singlet oxygen and to photodegrade into aldehyde-bearing fragments and, specifically, the dicarbonyls methylglyoxal and glyoxal that are responsible for cell damage (26, 75). This bisretinoid photodegradative process is responsible for the lower bisretinoid levels measured in light- *versus* dark-reared mice (35) and for the finding that mice burdened with age- and genotype (albino *Abca4*$^{-/-}$ mice)-associated increased bisretinoid (A2E and all-*trans*-retinal dimer) exhibit increased susceptibility to retina light damage (76). Similarly,

the accumulation of bisretinoids in photoreceptor cell outer segments with Mertk deficiency probably explains the light-associated retinal degeneration expressed by *Mertk*$^{-/-}$ mice.

Support for links among bisretinoid accumulation, adverse effects of light, and photoreceptor cell degeneration is provided by the evidence indicating that the rate of photoreceptor cell degeneration was more rapid in mice exposed to higher levels of intraocular light (albino *versus* agouti) and by the finding that ONL thinning in albino *Mertk*$^{-/-}$/Rpe65-Leu450 mice advanced more rapidly in inferior retina. Consistent with the premise that the light-associated effects of *Mertk* deficiency operate through bisretinoid was the observation that ONL thinning was more rapid in mice having higher levels of bisretinoid (Rpe65-Leu450 *versus* 450Met).

Based on work in the *Rdh8*$^{-/-}$/*Abca4*$^{-/-}$ mouse (77), it has been suggested that, apart from adverse effects of bisretinoids, all-*trans*-retinal is directly damaging to photoreceptor cells. In the *Mertk* mutant mouse, Abca4 and retinol dehydrogenases are functional; thus, all-*trans*-retinal does not accumulate. Rather, all-*trans*-retinal is reduced to nontoxic retinol, and the all-*trans*-retinal that escapes reduction forms bisretinoid. The difference between *Mertk* mutant mice and WT mice rests in the handling of the shed OS. Specifically, phagocytosis of the outer-segment debris is essential for photoreceptor cell survival. Of note, at 8 weeks of age, 11-*cis*-retinal levels are highest in agouti *Mertk*$^{-/-}$/Rpe65-Leu450 as compared with the two other *Mertk*$^{-/-}$ mouse lines (Fig. 5*D*). Thus, there is potential for release of more abundant all-*trans*-retinal in agouti *Mertk*$^{-/-}$/Rpe65-Leu450 mice, yet outer nuclear layer thickness is better preserved in these mice.

There are other apparently disparate retinal disorders that are accompanied by accumulations of autofluorescent material in the outer retina and/or in the subretinal space as in the *Mertk*$^{-/-}$ mice. For instance, in a mouse model of retinal detachment, outer-segment debris that is not phagocytosed by RPE becomes visible as foci of elevated autofluorescence (78). Within autofluorescence rings that often characterize fundus autofluorescence images in retinitis pigmentosa (79–83), photoreceptor cell viability is reduced, and qAF can be higher than at equivalent fundus positions in healthy eyes (84). Autofluorescent flecks visible in the fundus of STGD1 patients serve as yet another example. We have shown that fundus flecks in STGD1 are a manifestation of groups of degenerating photoreceptor cells (85). This conclusion is buttressed by the finding that flecks visualized in SW-AF images correspond to hyperreflective lesions extending radially within photoreceptor-attributable bands in spectral-domain OCT scans. The hyperreflectivity of flecks in spectral-domain OCT scans co-localizes with reduced or absent RPE melanin autofluorescence in NIR-AF images; loss of this signal is indicative of RPE atrophy. Abnormally increased SW-AF is also associated with outer segments that form the core of photoreceptor cell folds or rosettes in degenerating mouse retina (78, 86). As shown here in *Mertk*$^{-/-}$ mice, these findings indicate that the process of photoreceptor cell degeneration may involve increased bisretinoid formation. Under all of these conditions, the increased bisretinoid may have the potential to aggravate disease processes.

As was reported in human *MERTK*-associated disease (18), we observed hyperautofluorescent puncta in fundus SW-AF images of *Mertk*$^{-/-}$ mice. Similar granular-like hyperautofluorescent foci have been described in other mouse models of retinal degeneration (78, 87–93). In some cases, these foci have been assigned to hyperreflective lesions in the outer nuclear layer–attributable band of OCT scans and to circularly arranged ONL nuclei in histological sections (78), whereas in other work, it was suggested that macrophages within the subretinal space were the source of the hyperautofluorescence (18, 94, 95). In a mouse model of retinal detachment, we found that autofluorescent puncta visible in the fundus exhibited emission spectra (emission peaks at 581 and 629 nm with excitations at 488 and 561 nm, respectively) that were consistent with an origin from the bisretinoid fluorophores that form in photoreceptor cell outer segments (48, 78). In the present work, macrophages are unlikely to account for the hyperautofluorescent spots because F4/80 staining (Fig. 1*C*) is consistent with single cells rather than cell aggregates of a size sufficient to account for fundus spots.

Taken together, the more rapid photoreceptor cell degeneration in the *Mertk*$^{-/-}$ albino *versus* agouti mice on the same genetic background (*Mertk*$^{-/-}$/Rpe65-450Met) together with the faster degeneration in the *Mertk*$^{-/-}$/Rpe65-Leu450 *versus* 450Met mice (of the same albino coat color) are consistent with the premise that bisretinoid accumulation in the outer segments of *Mertk*$^{-/-}$ mice is responsible for light-mediated aggravation of photoreceptor cell degeneration. This work illustrates that photoreceptor cells can serve as an aberrant source of heightened fundus autofluorescence due to increased bisretinoid formation in impaired photoreceptor cells. These findings are not only relevant to human *MERTK* disease but are also relevant to our understanding of the paracentral rings of elevated AF in retinitis pigmentosa (96) and/or the bright AF flecks that characterize recessive Stargardt disease (44, 97).

Experimental procedures

Animals

Mice that were also homozygous for a targeted knockout of *Mertk* (*Mertk*$^{tm1Grl/J}$; *Mertk*$^{-/-}$) (Jackson Laboratory) were bred with albino C57BL/6J^{c2j} and 129SvJ mice to generate *Mertk*$^{-/-}$ albino mice that were homozygous for Rpe65-Leu450 or Rpe65-450Met and *Mertk*$^{-/-}$ agouti mice that were homozygous for Rpe65-450Met. Using genomic DNA isolated from tail tissue using the commercial KAPA Hot Start Mouse Genotyping kit (Kapa Biosystems) and primer sequences 5′-GCTTTAGCCTCCCCAGTAGC-3′ (forward; WT), 5′-TTTGCCAAGTTCTAATTCCATCAG-3′ (forward, knockout), and 5′-TTCCAAAGGCTACTGCGTGAAC-3′ (reverse, WT and knockout), WT and mutant *Mertk* alleles were amplified as 275- and 229-bp fragments, respectively. Mice were also genotyped for the Rpe65-L450M variant by PCR amplification (22) using primers 5′-ACCAGAAATTTGGAGGGAAAC-3′ (forward) and 5′-CCCTTCCATTCAGAGCTTCA-3′ (reverse). Digestion of the 545-bp product with MwoI restriction enzyme (New England Biolabs) yielded 180- and 365-bp fragments if the sequence corresponded to Leu-450 (WT) and an undigested

545 bp band if the sequence corresponded to the 450Met variant. Heterozygous mice exhibited all three bands. With Rpe65-450Met, Rpe65 protein levels are reduced (98), and we have shown that 450Met confers less A2E production than with Leu-450 (22). Mice were free of the *Rd8* mutation.

C57BL/6J (black, Rpe65-450Met variant) and C57BL/6J^{c2j} (B6(Cg)-Try<c-2J>/J, albino, Rpe65-450Met variant) mice were purchased from Jackson Laboratory as WT.

Pink-eyed inbred dystrophic (RCS) rats, black-eyed dystrophic RCS rats (RCS-*p*+), and pink-eyed congenic RCS-rdy+ rats that are WT at the rdy locus were obtained from Dr. Matthew LaVail and raised in a 12-h light/12-h dark environment at ~15 lux. The institutional animal care and use committee of Columbia University approved all procedures.

Fundus imaging

The pupils of anesthetized mice were dilated, the cornea was lubricated, and fundus autofluorescence images (55° wide-field lens; 0.98-mm detection pupil) were acquired with a confocal scanning laser ophthalmoscope (Spectralis HRA, Heidelberg Engineering, Heidelberg, Germany) (43). After visual pigment was bleached (20 s), laser power was set at ~280 microwatts and sensitivity at 100, nine successive frames were acquired at 488-nm excitation with the high-speed mode (138 images in 41 mice), and nonnormalized frames were saved. A mean of 100 frames were obtained at 790-nm excitation (sensitivity 105) with high-resolution ART (automatic real-time) mode and resized with Photoshop CS4 (Adobe Systems, San Jose, CA) to 768 × 768 pixels, the same as high-speed mode images. Near-IR reflectance images (820 nm) were also acquired. Mice were not serially imaged; each image was acquired from a different mouse.

qAF

As described (43), mean gray levels (GLs) were calculated from eight predefined segments around the optic disc, and blood vessels were excluded by histogram analysis. qAF at 488-nm excitation was calculated by normalization to the GL of the reference after subtraction of zero light (GL_0) and inclusion of a reference calibration factor. Fluorescence intensities at 790 nm were calculated by subtracting the minimal GL of optic nerve head measured by ImageJ (a public domain, Java-based image-processing program developed at the National Institutes of Health).

Quantitative HPLC and UPLC analysis

Mouse eyecups (4 eyes/sample, as indicated) were homogenized, extracted in chloroform/methanol (2:1), concentrated, and injected (30 μl) into the HPLC (Alliance System, Waters Corp., Milford, MA) using an Atlantis dC18 (3 μm, 4.6 × 150 mm; Waters) column as described (25) For UPLC quantitation, murine eyecup samples were redissolved in ethanol after extraction and injected (10 μl) into a Waters Acquity UPLC-MS system using an Acquity BEH Phenyl Column (1.7 μm, 2.1 × 100 mm; Waters) as described (35, 57). Rat posterior eyecups (2–6 eyecups/sample, as indicated) were homogenized, extracted with chloroform/methanol (2:1), and injected into an HPLC (Alliance System, Waters; with 2695 separation module, 2996 photodiode array detector, and 2475 multi-λ fluorescence detector). For analysis of A2E, all-*trans*-retinal dimer (atRAL dimer), and A2PE, dC18 (3 μm, 4.6 × 150 mm; Waters) and Delta Pak C4 (5 μm, 3.9 × 150 mm; Waters) columns were used as described (99).

For 11-*cis*-retinal quantification, mouse eyecups (1 eye/sample) were homogenized and derivatized using *O*-ethylhydroxylamine (100). Retinal *O*-ethyloxime was extracted with hexane and resuspended in acetonitrile. The Waters Acquity UPLC-MS system was used with a CSH C18 column (1.7 μm, 2.1 × 100 mm; Waters) and gradients of water (A) and acetonitrile (B) with 0.1% of formic acid as follows: beginning at 60% B, holding for 5 min, followed by a linear increase to 70% B over 55 min, followed by a linear increase to 100% B over 10 min (flow rate of 0.3 ml/min).

Histological analysis

Mouse eyes were marked with tissue dye and fixed (4% paraformaldehyde, 20% isopropyl alcohol, 2% TCA, and 2% zinc chloride), and 5-μm H&E-stained paraffin sections were prepared. The sections most centrally located within the ONH were imaged digitally. ONL width was measured at 200-μm intervals in the vertical plane and plotted as distance (mm) superior and inferior to the ONH. ONL area was calculated using the measurement interval of 0.2 mm multiplied by the sum of ONL thicknesses in superior and inferior hemiretina (ONH to 2.0 mm in superior and inferior hemiretina). To compare ONL thicknesses in superior *versus* inferior hemiretina, we calculated the mean of thicknesses measured at 0.2-mm intervals from the ONH to the position 2.0 mm in superior and inferior retina.

Fixed eyes were also mounted in Tissue-Tek O.C.T. compound (Sakura Finetek, Torrance, CA), and cryostat sections (10 μm; sagittal) through the ONH were stained with DAPI to label nuclei. Retina was examined under a fluorescence microscope (×40 objective; Zeiss Axioplan II microscope with AxioCam HRc camera; Carl Zeiss, Thornwood, NY) to detect DAPI-stained nuclei (359/461 nm, excitation/emission maxima) and autofluorescence (490/535 nm).

Statistical analysis

Statistical analysis was performed using GraphPad Prism version 6 (GraphPad Software, Inc., La Jolla, CA); $p < 0.05$ was considered significant.

Author contributions—J. Z., K. U., M. R., H. J. K., and J. R. S. data curation; J. Z., K. U., M. R., H. J. K., and J. R. S. formal analysis; J. Z., K. U., M. R., H. J. K., and J. R. S. validation; J. Z., K. U., H. J. K., and J. R. S. investigation; J. Z., K. U., M. R., H. J. K., and J. R. S. visualization; J. Z., K. U., and J. R. S. methodology; J. R. S. conceptualization; J. R. S. resources; J. R. S. software; J. R. S. supervision; J. R. S. funding acquisition; J. R. S. writing-original draft; J. R. S. project administration; J. R. S. writing-review and editing.

References

1. Prasad, D., Rothlin, C. V., Burrola, P., Burstyn-Cohen, T., Lu, Q., Garcia de Frutos, P., and Lemke, G. (2006) TAM receptor function in the retinal pigment epithelium. *Mol. Cell Neurosci.* **33,** 96–108

2. Duncan, J. L., LaVail, M. M., Yasumura, D., Matthes, M. T., Yang, H., Trautmann, N., Chappelow, A. V., Feng, W., Earp, H. S., Matsushima, G. K., and Vollrath, D. (2003) An RCS-like retinal dystrophy phenotype in mer knockout mice. *Invest. Ophthalmol. Vis. Sci.* **44,** 826–838 CrossRef Medline
3. Maddox, D. M., Hicks, W. L., Vollrath, D., LaVail, M. M., Naggert, J. K., and Nishina, P. M. (2011) An ENU-induced mutation in the Mertk gene (Mertknmf12) leads to a slow form of retinal degeneration. *Invest. Ophthalmol. Vis. Sci.* **52,** 4703–4709 CrossRef Medline
4. Dowling, J. E., and Sidman, R. L. (1962) Inherited retinal dystrophy in the rat. *J Cell Biol.* **14,** 73–109 CrossRef Medline
5. Bok, D., and Hall, M. O. (1971) The role of the pigment epithelium in the etiology of inherited retinal dystrophy in the rat. *J. Cell Biol.* **49,** 664–682 CrossRef Medline
6. LaVail, M. M., and Battelle, B.-A. (1975) Influence of eye pigmentation and light deprivation on inherited retinal dystrophy in the rat. *Exp. Eye Res.* **21,** 167–192 CrossRef Medline
7. Katz, M. L., Eldred, G. E., and Robison, W. G., Jr. (1987) Lipofuscin autofluorescence: evidence for vitamin A involvement in the retina. *Mech. Ageing Dev.* **39,** 81–90 CrossRef Medline
8. Organisciak, D. T., Li, M., Darrow, R. M., and Farber, D. B. (1999) Photoreceptor cell damage by light in young Royal College of Surgeons rats. *Curr. Eye Res.* **19,** 188–196 CrossRef Medline
9. Eldred, G. E. (1991) *The Fluorophores of the RCS Rat Retina and Implications for Retinal Degeneration*, CRC Press, Inc., Boca Raton, FL
10. Sparrow, J. R. (2007) RPE lipofuscin: formation, properties and relevance to retinal degeneration. In *Retinal Degenerations: Biology, Diagnostics and Therapeutics* (Tombran-Tink, J., and Barnstable, C. J., eds) pp. 213–236, Humana Press, Totowa, NJ
11. Mullen, R. J., and LaVail, M. M. (1976) Inherited retinal dystrophy: primary defect in pigment epithelium determined with experimental rat chimeras. *Science* **192,** 799–801 CrossRef Medline
12. Li, L. X., and Turner, J. E. (1988) Inherited retinal dystrophy in the RCS rat: prevention of photoreceptor degeneration by pigment epithelial cell transplantation. *Exp. Eye Res.* **47,** 911–917 CrossRef Medline
13. D'Cruz, P. M., Yasumura, D., Weir, J., Matthes, M. T., Abderrahim, H., LaVail, M. M., and Vollrath, D. (2000) Mutation of the receptor tyrosine kinase gene Mertk in the retinal dystrophic RCS rat. *Hum. Mol. Genet.* **9,** 645–651 CrossRef Medline
14. Feng, W., Yasumura, D., Matthes, M. T., LaVail, M. M., and Vollrath, D. (2002) MerTK triggers uptake of photoreceptor outer segments during phagocytosis by cultured retinal pigment epithelial cells. *J. Biol. Chem.* **277,** 17016–17022 CrossRef Medline
15. Vollrath, D., Feng, W., Duncan, J. L., Yasumura, D., D'Cruz, P. M., Chappelow, A., Matthes, M. T., Kay, M. A., and LaVail, M. M. (2001) Correction of the retinal dystrophy phenotype of the RCS rat by viral gene transfer of Mertk. *Proc. Natl. Acad. Sci. U.S.A.* **98,** 12584–12589 CrossRef Medline
16. Gal, A., Li, Y., Thompson, D. A., Weir, J., Orth, U., Jacobson, S. G., Apfelstedt-Sylla, E., and Vollrath, D. (2000) Mutations in MERTK, the human orthologue of the RCS rat retinal dystrophy gene, cause retinitis pigmentosa. *Nat. Genet.* **26,** 270–271 CrossRef Medline
17. Tschernutter, M., Jenkins, S. A., Waseem, N. H., Saihan, Z., Holder, G. E., Bird, A. C., Bhattacharya, S. S., Ali, R. R., and Webster, A. R. (2006) Clinical characterisation of a family with retinal dystrophy caused by mutation in the Mertk gene. *Br. J. Ophthalmol.* **90,** 718–723 CrossRef Medline
18. Charbel Issa, P., Bolz, H. J., Ebermann, I., Domeier, E., Holz, F. G., and Scholl, H. P. (2009) Characterisation of severe rod-cone dystrophy in a consanguineous family with a splice site mutation in the MERTK gene. *Br. J. Ophthalmol.* **93,** 920–925 CrossRef Medline
19. Sparrow, J. R., Gregory-Roberts, E., Yamamoto, K., Blonska, A., Ghosh, S. K., Ueda, K., and Zhou, J. (2012) The bisretinoids of retinal pigment epithelium. *Prog. Retin. Eye Res.* **31,** 121–135 CrossRef Medline
20. Sparrow, J. R. (2007) Lipofuscin of the retinal pigment epithelium. in *Atlas of Autofluorescence Imaging* (Holz, F. G., Schmitz-Valckenberg, S., Spaide, R. F., and Bird, A. C., eds) pp. 3–16, Springer, Heidelberg, Germany
21. Parish, C. A., Hashimoto, M., Nakanishi, K., Dillon, J., and Sparrow, J. (1998) Isolation and one-step preparation of A2E and iso-A2E, fluorophores from human retinal pigment epithelium. *Proc. Natl. Acad. Sci. U.S.A.* **95,** 14609–14613 CrossRef Medline
22. Kim, S. R., Fishkin, N., Kong, J., Nakanishi, K., Allikmets, R., and Sparrow, J. R. (2004) The Rpe65 Leu450Met variant is associated with reduced levels of the RPE lipofuscin fluorophores A2E and iso-A2E. *Proc. Natl. Acad. Sci. U.S.A.* **101,** 11668–11672 CrossRef Medline
23. Jang, Y. P., Matsuda, H., Itagaki, Y., Nakanishi, K., and Sparrow, J. R. (2005) Characterization of peroxy-A2E and furan-A2E photooxidation products and detection in human and mouse retinal pigment epithelial cell lipofuscin. *J. Biol. Chem.* **280,** 39732–39739 CrossRef Medline
24. Kim, S. R., Jang, Y. P., Jockusch, S., Fishkin, N. E., Turro, N. J., and Sparrow, J. R. (2007) The all-*trans*-retinal dimer series of lipofuscin pigments in retinal pigment epithelial cells in a recessive Stargardt disease model. *Proc. Natl. Acad. Sci. U.S.A.* **104,** 19273–19278 CrossRef Medline
25. Yamamoto, K., Yoon, K. D., Ueda, K., Hashimoto, M., and Sparrow, J. R. (2011) A novel bisretinoid of retina is an adduct on glycerophosphoethanolamine. *Invest. Ophthalmol. Vis. Sci.* **52,** 9084–9090 CrossRef Medline
26. Wu, Y., Yanase, E., Feng, X., Siegel, M. M., and Sparrow, J. R. (2010) Structural characterization of bisretinoid A2E photocleavage products and implications for age-related macular degeneration. *Proc. Natl. Acad. Sci.* **107,** 7275–7280 CrossRef Medline
27. Boyer, N. P., Higbee, D., Currin, M. B., Blakeley, L. R., Chen, C., Ablonczy, Z., Crouch, R. K., and Koutalos, Y. (2012) Lipofuscin and *N*-retinylidene-*N*-retinylethanolamine (A2E) accumulate in the retinal pigment epithelium in the absence of light exposure: their origin is 11-*cis*-retinal. *J. Biol. Chem.* **287,** 22276–22286 CrossRef Medline
28. Maeda, A., Maeda, T., Imanishi, Y., Kuksa, V., Alekseev, A., Bronson, J. D., Zhang, H., Zhu, L., Sun, W., Saperstein, D. A., Rieke, F., Baehr, W., and Palczewski, K. (2005) Role of photoreceptor-specific retinol dehydrogenase in the retinoid cycle *in vivo*. *J. Biol. Chem.* **280,** 18822–18832 CrossRef Medline
29. Ben-Shabat, S., Parish, C. A., Vollmer, H. R., Itagaki, Y., Fishkin, N., Nakanishi, K., and Sparrow, J. R. (2002) Biosynthetic studies of A2E, a major fluorophore of retinal pigment epithelial lipofuscin. *J. Biol. Chem.* **277,** 7183–7190 CrossRef Medline
30. Kim, S. R., He, J., Yanase, E., Jang, Y. P., Berova, N., Sparrow, J. R., and Nakanishi, K. (2007) Characterization of dihydro-A2PE: an intermediate in the A2E biosynthetic pathway. *Biochemistry* **46,** 10122–10129 CrossRef Medline
31. Sparrow, J. R., Nakanishi, K., and Parish, C. A. (2000) The lipofuscin fluorophore A2E mediates blue light-induced damage to retinal pigmented epithelial cells. *Invest. Ophthalmol. Vis. Sci.* **41,** 1981–1989 Medline
32. Sparrow, J. R., Vollmer-Snarr, H. R., Zhou, J., Jang, Y. P., Jockusch, S., Itagaki, Y., and Nakanishi, K. (2003) A2E-epoxides damage DNA in retinal pigment epithelial cells: vitamin E and other antioxidants inhibit A2E-epoxide formation. *J. Biol. Chem.* **278,** 18207–18213 CrossRef Medline
33. Kim, S. R., Nakanishi, K., Itagaki, Y., and Sparrow, J. R. (2006) Photooxidation of A2-PE, a photoreceptor outer segment fluorophore, and protection by lutein and zeaxanthin. *Exp. Eye Res.* **82,** 828–839 CrossRef Medline
34. Kim, S. R., Jang, Y. P., and Sparrow, J. R. (2010) Photooxidation of RPE Lipofuscin bisretinoids enhanced fluorescence intensity. *Vision Res.* **50,** 729–736 CrossRef Medline
35. Ueda, K., Zhao, J., Kim, H. J., and Sparrow, J. R. (2016) Photodegradation of retinal bisretinoids in mouse models and implications for macular degeneration. *Proc. Natl. Acad. Sci. U.S.A.* **113,** 6904–6909 CrossRef Medline
36. Wing, G. L., Blanchard, G. C., and Weiter, J. J. (1978) The topography and age relationship of lipofuscin concentration in the retinal pigment epithelium. *Invest. Ophthalmol. Vis. Sci.* **17,** 601–607 Medline
37. Feeney-Burns, L., Hilderbrand, E. S., and Eldridge, S. (1984) Aging human RPE: morphometric analysis of macular, equatorial, and peripheral cells. *Invest. Ophthalmol. Vis. Sci.* **25,** 195–200 Medline

38. Weiter, J. J., Delori, F. C., Wing, G. L., and Fitch, K. A. (1986) Retinal pigment epithelial lipofuscin and melanin and choroidal melanin in human eyes. *Invest. Ophthalmol. Vis. Sci.* **27,** 145–152 Medline
39. Mata, N. L., Weng, J., and Travis, G. H. (2000) Biosynthesis of a major lipofuscin fluorophore in mice and humans with ABCR-mediated retinal and macular degeneration. *Proc. Natl. Acad. Sci. U.S.A.* **97,** 7154–7159 CrossRef Medline
40. Delori, F. C., Goger, D. G., and Dorey, C. K. (2001) Age-related accumulation and spatial distribution of lipofuscin in RPE of normal subjects. *Invest. Ophthalmol. Vis. Sci.* **42,** 1855–1866 Medline
41. Greenberg, J. P., Duncker, T., Woods, R. L., Smith, R. T., Sparrow, J. R., and Delori, F. C. (2013) Quantitative fundus autofluorescence in healthy eyes. *Invest. Ophthalmol. Vis. Sci.* **54,** 5684–5693 CrossRef Medline
42. Charbel Issa, P., Singh, M. S., Lipinski, D. M., Chong, N. V., Delori, F. C., Barnard, A. R., and MacLaren, R. E. (2012) Optimization of *in vivo* confocal autofluorescence imaging of the ocular fundus in mice and its application to models of human retinal degeneration. *Invest. Ophthalmol. Vis. Sci.* **53,** 1066–1075 CrossRef Medline
43. Sparrow, J. R., Blonska, A., Flynn, E., Duncker, T., Greenberg, J. P., Secondi, R., Ueda, K., and Delori, F. C. (2013) Quantitative fundus autofluorescence in mice: correlation with HPLC quantitation of RPE lipofuscin and measurement of retina outer nuclear layer thickness. *Invest. Ophthalmol. Vis. Sci.* **54,** 2812–2820 CrossRef Medline
44. Eagle, R. C., Jr., Lucier, A. C., Bernardino, V. B., Jr., and Yanoff, M. (1980) Retinal pigment epithelial abnormalities in fundus flavimaculatus. *Ophthalmology* **87,** 1189–1200 CrossRef Medline
45. Delori, F. C., Staurenghi, G., Arend, O., Dorey, C. K., Goger, D. G., and Weiter, J. J. (1995) *In vivo* measurement of lipofuscin in Stargardt's disease–Fundus flavimaculatus. *Invest. Ophthalmol. Vis. Sci.* **36,** 2327–2331 Medline
46. Burke, T. R., Duncker, T., Woods, R. L., Greenberg, J. P., Zernant, J., Tsang, S. H., Smith, R. T., Allikmets, R., Sparrow, J. R., and Delori, F. C. (2014) Quantitative fundus autofluorescence in recessive Stargardt disease. *Invest. Ophthalmol. Vis. Sci.* **55,** 2841–2852 CrossRef Medline
47. Weng, J., Mata, N. L., Azarian, S. M., Tzekov, R. T., Birch, D. G., and Travis, G. H. (1999) Insights into the function of Rim protein in photoreceptors and etiology of Stargardt's disease from the phenotype in abcr knockout mice. *Cell* **98,** 13–23 CrossRef Medline
48. Sparrow, J. R., Wu, Y., Nagasaki, T., Yoon, K. D., Yamamoto, K., and Zhou, J. (2010) Fundus autofluorescence and the bisretinoids of retina. *Photochem. Photobiol. Sci.* **9,** 1480–1489 CrossRef Medline
49. Herron, W. L., Riegel, B. W., Myers, O. E., and Rubin, M. L. (1969) Retinal dystrophy in the rat–a pigment epithelial disease. *Invest. Ophthalmol.* **8,** 595–604 Medline
50. Delmelle, M., Noell, W. K., and Organisciak, D. T. (1975) Hereditary retinal dystrophy in the rat: rhodopsin, retinol, vitamin A deficiency. *Exp. Eye Res.* **21,** 369–380 CrossRef Medline
51. LaVail, M. M., Pinto, L. H., and Yasumura, D. (1981) The interphotoreceptor matrix in rats with inherited retinal dystrophy. *Invest. Ophthalmol. Vis. Sci.* **21,** 658–668 Medline
52. Lolley, R. N., and Farber, D. B. (1976) A proposed link between debris accumulation, guanosine 3′,5′ cyclic monophosphate changes and photoreceptor cell degeneration in retina of RCS rats. *Exp. Eye Res.* **22,** 477–486 CrossRef Medline
53. Burden, E. M., Reading, H. W., and Yates, C. M. (1971) An investigation into the structural integrity of lysosomes and its effect in the normal and dystrophic rat retina. *Exp. Eye Res.* **11,** 140 CrossRef Medline
54. Paavo, M., Zhao, J., Kim, H. J., Lee, W., Zernant, J., Cai, C., Allikmets, R., Tsang, S. H., and Sparrow, J. R. (2018) Mutations in GPR143/OA1 and ABCA4 inform interpretations of short-wavelength and near-infrared fundus autofluorescence. *Invest. Ophthalmol. Vis. Sci.* **59,** 2459–2469 CrossRef Medline
55. Matthes, M. T., and LaVail, M. M. (1989) Inherited retinal dystrophy in the RCS rat: composition of the outer segment debris zone. *Prog. Clin. Biol. Res.* **314,** 315–330 Medline
56. Koh, S., Chen, W. J., Dejneka, N. S., Harris, I. R., Lu, B., Girman, S., Saylor, J., Wang, S., and Eroglu, C. (2018) Subretinal human umbilical tissue-derived cell transplantation preserves retinal synaptic connectivity and attenuates Müller glial reactivity. *J. Neurosci.* **38,** 2923–2943 CrossRef Medline
57. Kim, H. J., and Sparrow, J. R. (2018) Novel bisretinoids of human retina are lyso alkyl-ether glycerophosphoethanolamine-bearing A2PE species. *J. Lipid Res.* **59,** 1620–1629 CrossRef Medline
58. Nagasaki, T., and Zhao, J. (2003) Centripetal movement of corneal epithelial cells in the normal adult mouse. *Invest. Ophthalmol. Vis. Sci.* **44,** 558–566 CrossRef Medline
59. Maeda, A., Golczak, M., Chen, Y., Okano, K., Kohno, H., Shiose, S., Ishikawa, K., Harte, W., Palczewska, G., Maeda, T., and Palczewski, K. (2011) Primary amines protect against retinal degeneration in mouse models of retinopathies. *Nat. Chem. Biol.* **8,** 170–178 CrossRef Medline
60. Wu, Y., Fishkin, N. E., Pande, A., Pande, J., and Sparrow, J. R. (2009) Novel lipofuscin bisretinoids prominent in human retina and in a model of recessive Stargardt disease. *J. Biol. Chem.* **284,** 20155–20166 CrossRef Medline
61. Salvador, G. A., and Giusto, N. M. (1998) Characterization of phospholipase D activity in bovine photoreceptor membranes. *Lipids* **33,** 853–860 CrossRef Medline
62. Anderson, R. E., and Maude, M. B. (1970) Phospholipids of bovine outer segments. *Biochemistry* **9,** 3624–3628 CrossRef Medline
63. Strick, D. J., and Vollrath, D. (2010) Focus on molecules: MERTK. *Exp. Eye Res.* **91,** 786–787 CrossRef Medline
64. McHenry, C. L., Liu, Y., Feng, W., Nair, A. R., Feathers, K. L., Ding, X., Gal, A., Vollrath, D., Sieving, P. A., and Thompson, D. A. (2004) MERTK arginine-844-cysteine in a patient with severe rod-cone dystrophy: loss of mutant protein function in transfected cells. *Invest. Ophthalmol. Vis. Sci.* **45,** 1456–1463 CrossRef Medline
65. Battelle, B. A., and LaVail, M. M. (1978) Rhodopsin content and rod outer segment length in albino rat eyes: modification by dark adaptation. *Exp. Eye Res.* **26,** 487–497 CrossRef Medline
66. Nusinowitz, S., Nguyen, L., Radu, R., Kashani, Z., Farber, D., and Danciger, M. (2003) Electroretinographic evidence for altered phototransduction gain and slowed recovery from photobleaches in albino mice with a MET450 variant in RPE6. *Exp. Eye Res.* **77,** 627–638 CrossRef Medline
67. Wenzel, A., Reme, C. E., Williams, T. P., Hafezi, F., and Grimm, C. (2001) The Rpe65 Leu450Met variation increases retinal resistance against light-induced degeneration by slowing rhodopsin regeneration. *J. Neurosci.* **21,** 53–58 CrossRef Medline
68. Danciger, M., Matthes, M. T., Yasamura, D., Akhmedov, N. B., Rickabaugh, T., Gentleman, S., Redmond, T. M., La Vail, M. M., and Farber, D. B. (2000) A QTL on distal chromosome 3 that influences the severity of light-induced damage to mouse photoreceptors. *Mamm. Genome* **11,** 422–427 CrossRef Medline
69. Wenzel, A., Grimm, C., Samardzija, M., and Remé, C. E. (2003) The genetic modified Rpe65Leu$_{450}$: effect on light damage susceptibility in c-Fos-deficient mice. *Invest. Ophthalmol. Vis. Sci.* **44,** 2798–2802 CrossRef Medline
70. Hao, W., Wenzel, A., Obin, M. S., Chen, C. K., Brill, E., Krasnoperova, N. V., Eversole-Cire, P., Kleyner, Y., Taylor, A., Simon, M. I., Grimm, C., Reme, C., Remé, C. E., and Lem, J. (2002) Evidence for two apoptotic pathways in light-induced retinal degeneration. *Nat. Genet.* **32,** 254–260 CrossRef Medline
71. Herron, W. L., Jr, Riegel, B. W., Brennan, E., and Rubin, M. L. (1974) Retinal dystrophy in the pigmented rat. *Invest. Ophthalmol.* **13,** 87–94 Medline
72. Penn, J. S., and Williams, T. P. (1986) Photostasis: regulation of daily photon-catch by rat retinas in response to various cyclic illuminances. *Exp. Eye Res.* **43,** 915–928 CrossRef Medline
73. Naash, M. L., Peachey, N. S., Li, Z.-Y., Gryczan, C. C., Goto, Y., Blanks, J., Milam, A. H., and Ripps, H. (1996) Light-induced acceleration of photoreceptor degeneration in transgenic mice expressing mutant rhodopsin. *Invest. Ophthalmol. Vis. Sci.* **37,** 775–782 Medline
74. Heckenlively, J. R., Rodriguez, J. A., and Daiger, S. P. (1991) Autosomal dominant sectoral retinitis pigmentosa: two families with transversion mutation in codon 23 of rhodopsin. *Arch. Ophthalmol.* **109,** 84–91 CrossRef Medline

75. Yoon, K. D., Yamamoto, K., Ueda, K., Zhou, J., and Sparrow, J. R. (2012) A novel source of methylglyoxal and glyoxal in retina: implications for age-related macular degeneration. *PLoS One* **7,** e41309 CrossRef Medline
76. Wu, L., Nagasaki, T., and Sparrow, J. R. (2010) Photoreceptor cell degeneration in *Abcr*$^{-/-}$ mice. *Adv. Exp. Med. Biol.* **664,** 533–539 CrossRef Medline
77. Maeda, A., Maeda, T., Golczak, M., and Palczewski, K. (2008) Retinopathy in mice induced by disrupted all-*trans*-retinal clearance. *J. Biol. Chem.* **283,** 26684–26693 CrossRef Medline
78. Secondi, R., Kong, J., Blonska, A. M., Staurenghi, G., and Sparrow, J. R. (2012) Fundus autofluorescence findings in a mouse model of retinal detachment. *Invest. Ophthalmol. Vis. Sci.* **53,** 5190–5197 CrossRef Medline
79. Robson, A. G., El-Amir, A., Bailey, C., Egan, C. A., Fitzke, F. W., Webster, A. R., Bird, A. C., and Holder, G. E. (2003) Pattern ERG correlates of abnormal fundus autofluorescence in patients with retinitis pigmentosa and normal visual acuity. *Invest. Ophthalmol. Vis. Sci.* **44,** 3544–3550 CrossRef Medline
80. Duncker, T., Tabacaru, M. R., Lee, W., Tsang, S. H., Sparrow, J. R., and Greenstein, V. C. (2013) Comparison of near-infrared and short-wavelength autofluorescence in retinitis pigmentosa. *Invest. Ophthalmol. Vis. Sci.* **54,** 585–591 CrossRef Medline
81. von Rückmann, A., Fitzke, F. W., and Bird, A. C. (1999) Distribution of pigment epithelium autofluorescence in retinal disease state recorded *in vivo* and its change over time. *Graefes Arch. Clin. Exp. Ophthalmol.* **237,** 1–9 CrossRef Medline
82. Popović, P., Jarc-Vidmar, M., and Hawlina, M. (2005) Abnormal fundus autofluorescence in relation to retinal function in patients with retinitis pigmentosa. *Graefes Arch. Clin. Exp. Ophthalmol.* **243,** 1018–1027 CrossRef Medline
83. Aizawa, S., Mitamura, Y., Hagiwara, A., Sugawara, T., and Yamamoto, S. (2010) Changes of fundus autofluorescence, photoreceptor inner and outer segment junction line, and visual function in patients with retinitis pigmentosa. *Clin. Exp. Ophthalmol.* **38,** 597–604 CrossRef Medline
84. Schuerch, K., Woods, R. L., Lee, W., Duncker, T., Delori, F. C., Allikmets, R., Tsang, S. H., and Sparrow, J. R. (2017) Quantifying fundus autofluorescence in patients with retinitis pigmentosa. *Invest. Ophthalmol. Vis. Sci.* **58,** 1843–1855 CrossRef Medline
85. Sparrow, J. R., Marsiglia, M., Allikmets, R., Tsang, S., Lee, W., Duncker, T., and Zernant, J. (2015) Flecks in recessive Stargardt disease: short-wavelength autofluorescence, near-infrared autofluorescence, and optical coherence tomography. *Invest. Ophthalmol. Vis. Sci.* **56,** 5029–5039 CrossRef Medline
86. Flynn, E., Ueda, K., Auran, E., Sullivan, J. M., and Sparrow, J. R. (2014) Fundus autofluorescence and photoreceptor cell rosettes in mouse models. *Invest. Ophthalmol. Vis. Sci.* **55,** 5643–5652 CrossRef Medline
87. Huber, G., Beck, S. C., Grimm, C., Sahaboglu-Tekgoz, A., Paquet-Durand, F., Wenzel, A., Humphries, P., Redmond, T. M., Seeliger, M. W., and Fischer, M. D. (2009) Spectral domain optical coherence tomography in mouse models of retinal degeneration. *Invest. Ophthalmol. Vis. Sci.* **50,** 5888–5895 CrossRef Medline
88. Seeliger, M. W., Beck, S. C., Pereyra-Muñoz, N., Dangel, S., Tsai, J. Y., Luhmann, U. F., van de Pavert, S. A., Wijnholds, J., Samardzija, M., Wenzel, A., Zrenner, E., Narfström, K., Fahl, E., Tanimoto, N., Acar, N., and Tonagel, F. (2005) In vivo confocal imaging of the retina in animal models using scanning laser ophthalmoscopy. *Vision Res.* **45,** 3512–3519 CrossRef Medline
89. Zhou, Y., Sheets, K. G., Knott, E. J., Regan, C. E., Jr., Tuo, J., Chan, C. C., Gordon, W. C., and Bazan, N. G. (2011) Cellular and 3D optical coherence tomography assessment during the initiation and progression of retinal degeneration in the Ccl2/Cx3cr1-deficient mouse. *Exp. Eye Res.* **93,** 636–648 CrossRef Medline
90. Wang, N. K., Fine, H. F., Chang, S., Chou, C. L., Cella, W., Tosi, J., Lin, C. S., Nagasaki, T., and Tsang, S. H. (2009) Cellular origin of fundus autofluorescence in patients and mice with a defective *NR2E3* gene. *Br. J. Ophthalmol.* **93,** 1234–1240 CrossRef Medline
91. Xu, H., Chen, M., Manivannan, A., Lois, N., and Forrester, J. V. (2008) Age-dependent accumulation of lipofuscin in perivascular and subretinal microglia in experimental mice. *Aging Cell* **7,** 58–68 CrossRef Medline
92. Dunaief, J. L., Dentchev, T., Ying, G. S., and Milam, A. H. (2002) The role of apoptosis in age-related macular degeneration. *Arch. Ophthalmol.* **120,** 1435–1442 CrossRef Medline
93. Chen, X., Kezic, J., Bernard, C., and McMenamin, P. G. (2013) Rd8 mutation in the Crb1 gene of CD11c-eYFP transgenic reporter mice results in abnormal numbers of CD11c-positive cells in the retina. *J. Neuropathol. Exp. Neurol.* **72,** 782–790 CrossRef Medline
94. Wang, J., Ohno-Matsui, K., Yoshida, T., Shimada, N., Ichinose, S., Sato, T., Mochizuki, M., and Morita, I. (2009) Amyloid-β up-regulates complement factor B in retinal pigment epithelial cells through cytokines released from recruited macrophages/microglia: another mechanism of complement activation in age-related macular degeneration. *J. Cell. Physiol.* **220,** 119–128 CrossRef Medline
95. Akhmedov, N. B., Piriev, N. I., Chang, B., Rapoport, A. L., Hawes, N. L., Nishina, P. M., Nusinowitz, S., Heckenlively, J. R., Roderick, T. H., Kozak, C. A., Danciger, M., Davisson, M. T., and Farber, D. B. (2000) A deletion in a photoreceptor-specific nuclear receptor mRNA causes retinal degeneration in the rd7 mouse. *Proc. Natl. Acad. Sci. U.S.A.* **97,** 5551–5556 CrossRef Medline
96. Robson, A. G., Michaelides, M., Luong, V. A., Holder, G. E., Bird, A. C., Webster, A. R., Moore, A. T., and Fitzke, F. W. (2008) Functional correlates of fundus autofluorescence abnormalities in patients with RPGR or RIMS1 mutations causing cone or cone rod dystrophy. *Br. J. Ophthalmol.* **92,** 95–102 CrossRef Medline
97. Cukras, C. A., Wong, W. T., Caruso, R., Cunningham, D., Zein, W., and Sieving, P. A. (2012) Centrifugal expansion of fundus autofluorescence patterns in Stargardt disease over time. *Arch. Ophthalmol.* **130,** 171–179 CrossRef Medline
98. Lyubarsky, A. L., Savchenko, A. B., Morocco, S. B., Daniele, L. L., Redmond, T. M., and Pugh, E. N. (2005) Mole quantity of RPE65 and its productivity in the generation of 11-*cis*-retinal from retinyl esters in the living mouse eye. *Biochemistry* **44,** 9880–9888 CrossRef Medline
99. Sparrow, J. R., Kim, S. R., and Wu, Y. (2010) Experimental approaches to the study of A2E, a bisretinoid lipofuscin chromophore of retinal pigment epithelium. *Methods Mol. Biol.* **652,** 315–327 CrossRef Medline
100. Kane, M. A., Folias, A. E., and Napoli, J. L. (2008) HPLC/UV quantitation of retinal, retinol, and retinyl esters in serum and tissues. *Anal. Biochem.* **378,** 71–79 CrossRef Medline